Science Advances
AAAS

advances.sciencemag.org/cgi/content/full/6/29/eabb1421/DC1

Supplementary Materials for

An artificial metalloenzyme for catalytic cancer-specific DNA cleavage and operando imaging

Liang Gao, Ya Zhang, Lina Zhao*, Wenchao Niu, Yuhua Tang, Fuping Gao, Pengju Cai, Qing Yuan, Xiayan Wang, Huaidong Jiang, Xueyun Gao*

*Corresponding author. Email: gaoxy@ihep.ac.cn (X.G.); linazhao@ihep.ac.cn (L.Z.)

Published 15 July 2020, *Sci. Adv.* **6**, eabb1421 (2020)
DOI: 10.1126/sciadv.abb1421

This PDF file includes:

1. Determination of RGD-BSA-CuCs and BSA-CuCs concentration by ICP-MS analysis

The concentration of RGD-BSA-CuCs and BSA-CuCs were evaluated by ICP-MS analysis (Thermo Elemental X7, USA). Firstly, the purified RGD-BSA-CuCs or BSA-CuCs were digested by mixed H_2O_2 and HNO_3 at a volume ratio of 1:3 over night. Then the solution was evaporated to about 0.3 mL and further diluted by 2% HNO_3 to final 5.0 mL. Calibration plot for standard Cu was profiled by injecting a series of standard aqueous Cu solutions (0.1, 0.5, 1, 5, 10, 50, 100 ng mL^{-1} containing 2% HNO_3) into ICP-MS system. Then completely digested RGD-BSA-CuCs or BSA-CuCs solution was followed by the standard Cu to measure cluster concentration in above samples. The final mineralization ratios of Cu in RGD-BSA-CuCs or BSA-CuCs are determined around 55%. Each experiment was conducted in triplicate.

2. Calculation of the orientation of Cu_{13} core stuck in BSA by docking calculation

We utilized molecular docking calculation to figure out the orientation of Cu_{13} core stuck in BSA. First, the geometry of Cu_{13} core was optimized by DFT calculation as shown in Fig. 2E (right image). Second, BSA configuration was exported from pdbbank with ID as 4F5S. The AutoDock 4.2 package (*29, 30*) was used to find the binding site of Cu_{13} core in BSA and the orientation of Cu_{13} core exposed. We performed a global docking of Cu_{13} core on BSA surface with all bonds being rigid. The Cu_{13} core was found to bind in the pocket composed by Helix 65-75, Helix 97-103 and the turn between Helix 226-246 and Helix 248-266 on the interface between Domain I and II of BSA (fig. S1, B and C). The Cu_{13} core was stably stuck by His67 and His346 residues with imidazolyl group through coordination bond, and Asp248, Glu243 and Glu251 residues in negative charged through electrostatic interaction (fig. S1D). The electron cloud overlap is described in detail between the Cu_{13} core and these contacted residues, which support the stable stuck of Cu_{13} core in the surficial pocket of BSA.

3. Determination of the Fermi level of clusters

The optical band gap E_g, can be calculated by the Tauc's approach applied for semiconductors, (αhv) =

$A(h\nu - E_g)^n$, where α is the absorption coefficient, h is Plank constant, ν is the frequency of the radiation, A is a constant, and n = 1/2 because clusters are intrinsic semiconductors (*26*). The E_g value of BSA-CuCs obtained from the Tauc's fitting is in the range of 3.01−3.74 eV, and that of RGD-BSA-CuCs is in the range of 2.89−3.64 eV (fig. S2).

Subsequently, the Fermi level of Cu clusters can be described by a theoretical prediction previously reported (*26*), that is, $E_{F\ \mathrm{CuCs}} = -E_{F\,\mathrm{Cu\ bulk}} + 0.95 \times \frac{E_{g\ \mathrm{CuCs}}}{E_{F\ \mathrm{Cu\ bulk}}}$, where $E_{F\,\mathrm{Cu\ bulk}} = 7$ eV is the Fermi energy of the bulk copper. The detailed calculations are listed as following,

For BSA-CuCs:

$$E_{F\ \mathrm{BSA\text{-}CuCs}} = -E_{F\,\mathrm{Cu\ bulk}} + 0.95 \times \frac{E_{g\ \mathrm{BSA\text{-}CuCs}}}{E_{F\ \mathrm{Cu\ bulk}}} = -7 + 0.95 \times (3.01/7) = -6.6\ e\mathrm{V} \quad (1)$$

$$E_{F\ \mathrm{BSA\text{-}CuCs}} = -E_{F\,\mathrm{Cu\ bulk}} + 0.95 \times \frac{E_{g\ \mathrm{BSA\text{-}CuCs}}}{E_{F\ \mathrm{Cu\ bulk}}} = -7 + 0.95 \times (3.74/7) = -6.5\ e\mathrm{V} \quad (2)$$

For RGD-BSA-CuCs:

$$E_{F\ \mathrm{RGD\text{-}BSA\text{-}CuCs}} = -E_{F\,\mathrm{Cu\ bulk}} + 0.95 \times \frac{E_{g\ \mathrm{RGD\text{-}BSA\text{-}CuCs}}}{E_{F\ \mathrm{Cu\ bulk}}} = -7 + 0.95 \times (2.89/7) = -6.6\ e\mathrm{V} \quad (3)$$

$$E_{F\ \mathrm{RGD\text{-}BSA\text{-}CuCs}} = -E_{F\,\mathrm{Cu\ bulk}} + 0.95 \times \frac{E_{g\ \mathrm{RGD\text{-}BSA\text{-}CuCs}}}{E_{F\ \mathrm{Cu\ bulk}}} = -7 + 0.95 \times (3.64/7) = -6.5\ e\mathrm{V} \quad (4)$$

4. Steady-State Kinetic Analysis of Peroxidase-Like RGD-BSA-CuCs

Steady-state kinetic assays were carried out at 37 °C in a 96-well plate. Chemicals were added into 200 μL of buffer solution containing 12 μM RGD-BSA-CuCs, 25 μM Amplex UltraRed and a series concentration of H_2O_2 (from 50 μM to 500 μM) at pH 6.5 or 7.4. Kinetic measurements were conducted by monitoring the fluorescence change of oxidized Amplex UltraRed at 585 nm in a time scan mode

during the first 30 min.

Catalytic parameters were determined by fitting data to the Michaelis−Menten equation (Equation (5)) (*45*). In this equation, ν is the initial velocity of conversion, V_{max} is the maximum rate of conversion, [S] is the substrate concentration, and K_m is the apparent Michaelis–Menten constant. Practically, the initial velocity of •OH formation can be converted to the initial velocity of oxidized Amplex UltraRed fluorescence promotion *via* Equation (6). To be more specific, if through oxidized Amplex UltraRed dilute solution, that less than 5% of the excitation energy is absorbed, the fluorescence measurement can be used to evaluate the concentration of oxidized Amplex UltraRed. In Equation (6), I_f is the fluorescence emission intensity of oxidized Amplex UltraRed, k is a proportionality constant, b is the optical path length, and c is the concentration of oxidized Amplex UltraRed. Furthermore, to determine K_m and V_{max}, Lineweaver–Burk plot was obtained as given (Equation (7)). Additionally, catalytic constant (K_{cat}) can be calculated from V_{max} divided by clusters' molar concentration [E] (Equation (8)).

$$v = \frac{V_{\max}[S]}{K_m + [S]} \quad (5)$$

$$I_f = kbc \quad (6)$$

$$\frac{1}{v} = \frac{K_m}{V_{\max}[S]} + \frac{1}{V_{\max}} \quad (7)$$

$$K_{cat} = \frac{V_{\max}}{[E]} \quad (8)$$

5. Characterization of RGD-BSA-CuCs before and after catalysis by XPS and AES

Firstly, 12 μM RGD-BSA-CuCs incubated with 100 μM H_2O_2 in pH 6.5 or 7.4 buffer solution were mixed at 37 °C for 24 h. Then samples were rinsed and concentrated before leaving a drop of equivoluminal solution on a piece of silicon wafer, drying by vacuum pumping, and immediately introducing the samples into the XPS prechamber under high vacuum condition. XPS and AES characterization were performed on a Thermo Scientific ESCALab 250Xi using 200 W monochromated

Al Kα radiation. The 500 μm X-ray spot was employed for XPS analysis. The base pressure in the analysis chamber was about 3×10^{-9} mbar. Typically, the hydrocarbon C1s line at 284.8 eV from adventitious carbon is utilized for energy referencing. Detailed XPS scans recorded for Cu 2p region are located between 920 eV and 970 eV, while that of AES scans for Cu LMM region were recorded between 555 eV and 585 eV. The atomic ratios of Cu (0), Cu (I) and Cu (II) in RGD-BSA-CuCs were estimated by calculating the area under each peak after subtracting of the base line. The corresponding results of aqueous solution containing 12 μM RGD-BSA-CuCs at pH 6.5 or 7.4 were set as controls.

6. Specificity investigation of RGD-BSA-CuCs targeting integrin on A549 cell membrane

A549 cells were first split into a glass bottomed culture dish designed especially for confocal laser scanning microscopy (CLSM) observation, and incubated in the culture media to allow 70% confluence overnight. Then 39 μM RGD-BSA-CuCs suspension was cocultured with cells for 3 h, and then cells were washed for three times. Then they were stained with commercial lysosome fluorescent dye (LysoTracker Red DND-99) before immediate observation with a 60×objective of CLSM (Olympus, FV1000MPE, Japan). Blue fluorescence excited by 405 nm laser shows the distribution of RGD-BSA-CuCs in A549 cells, while the fluorescence of lysosome probe was collected mainly in red channel when excited by 559 nm laser. The cells without any treatment, treated with 39 μM BSA-CuCs, or pretreated with 2.0 mM RGD peptide for 1 h followed by 39 μM RGD-BSA-CuCs were set as controls. The images were collected at the same setting as above.

7. Quantitative analysis of Cu content in single A549 cell *via* ICP-MS

A549 cells were reseeded in 6-well plate at a population of 6×10^5 and were allowed proliferation for 24 h. After incubated with 19 μM RGD-BSA-CuCs or BSA-CuCs for 24 h, the cells were washed to remove free clusters and counted by flow cytometry (Accuri C6, BD, USA) before pre-digested by mixed acid ($V_{H_2O_2}$: V_{HNO_3} at a volume ratio of 1:3) over night. Then the samples were diluted by 2% HNO_3 to a final volume. The procedures to obtain Cu standard calibration plot and measure Cu content in each sample were described above. Each experiment was repeated three times.

The concentration of Cu atoms enveloped by single A549 cell was calculated by dividing the concentration of total internalized Cu atoms by the number of cells. The average concentration of Cu atoms in a single A549 cell can be calculated by the following equation.

For BSA-CuCs:

$$c = \frac{\rho V}{M_{\mathrm{Cu}} n_{\mathrm{cell}} V_{\mathrm{cell}}} = \frac{5.5 \times 10^{-6} \times 5.0 \times 10^{-3}}{64 \times 5.0 \times 10^{5} \times 7 \times 10^{-12}} = 1.2 \times 10^{-4} \qquad (9)$$

For RGD-BSA-CuCs:

$$c = \frac{\rho V}{M_{\mathrm{Cu}} n_{\mathrm{cell}} V_{\mathrm{cell}}} = \frac{7.2 \times 10^{-6} \times 5.0 \times 10^{-3}}{64 \times 5.0 \times 10^{5} \times 7 \times 10^{-12}} = 1.6 \times 10^{-4} \qquad (10)$$

c: average concentration of Cu atoms in a single A549 cell (M)

ρ: mass concentration of Cu ions from ICP-MS analysis (g L^{-1})

V: ultimate volume of the analyzed solution (L)

M_{Cu}: relative atomic mass of Cu (g mol^{-1})

n_{cell}: number of A549 cells

V_{cell}: volume of single A549 cell

8. RGD-BSA-CuCs' *in vivo* targeting capability

BALB/c nude mice were subcutaneously injected in the right flank with 1×10^7 A549 cells, and tumors were allowed to grow to 100 mm^3. Mice were randomly assigned into two groups (n = 3 for each group) before intraperitoneally (i.p.) administrated with 200 μL of RGD-BSA-CuCs or BSA-CuCs at Cu dose of 2.5 mg kg^{-1}. Animals were sacrificed by cervical dislocation at 1 and 2 h post-injection, respectively. Tumors were collected, freeze-dried, weighed, and digested by mixed acid. Then the Cu content was analyzed by ICP-MS measurement mentioned above.

9. Pharmacokinetics and biodistributions of RGD-BSA-CuCs

BALB/c nude mice were subcutaneously injected in the right flank with 1×10^7 A549 cells, and tumors were allowed to grow to 100 mm^3. Mice were randomly assigned into ten groups (n = 3 for each group) before they were i.p. administrated with 200 μL of RGD-BSA-CuCs at Cu dose of 2.5 mg kg^{-1}. Animals were sacrificed (three per time point) at 5 min, 15 min, 30 min, 1 h, 2 h, 4 h, 6 h, 12 h and 24 h after clusters administration. Then mice's blood, hearts, livers, spleens, lungs, kidneys, and tumors were harvested. Blood samples were directly digested by mixed acid ($V_{H_2O_2}$: V_{HNO_3} at a volume ratio of 1:3). The organs and tumors were collected, freeze-dried, weighed, and digested by the same procedure. Then the digested samples were diluted by 2% HNO_3 to a final volume before Cu content was analyzed by ICP-MS. The blood distribution half-life ($t_{1/2\alpha}$) and blood clearance half-life ($t_{1/2\beta}$) of Cu clusters are fitted by two compartment model through software DAS 2.0.

10. Histopathological analysis and biochemistry test

At the end of therapeutic period, the mice were sacrificed. Their major organs (heart, liver, spleen, lung, and kidney) and blood were then collected for pathological and biochemistry studies, respectively. The major organs were fixed in 10% formalin, embedded in paraffin, sectioned, and then stained by hematoxylin and eosin. The stained tissue sections were then observed using NanoZoomer digital pathology system (Hamamatsu, Japan) to monitor the possible histological changes. The liver function related alanine aminotransferase (ALT), aspartate aminotransferase (AST), alkaline phosphatase (ALP), and nephrotoxicity indicator creatinine (CREA), along with the blood panel parameters including white blood cells (WBC), red blood cells (RBC), hemoglobin (HGB), hematocrit (HCT), mean corpuscular volume (MCV), mean corpuscular hemoglobin (MCH), mean corpuscular hemoglobin concentration (MCHC), lymphocyte (LYM), and red blood cell distribution width-standard deviation (RDW-SD) were measured using standard hematology test.

11. Supplementary Figures and Tables

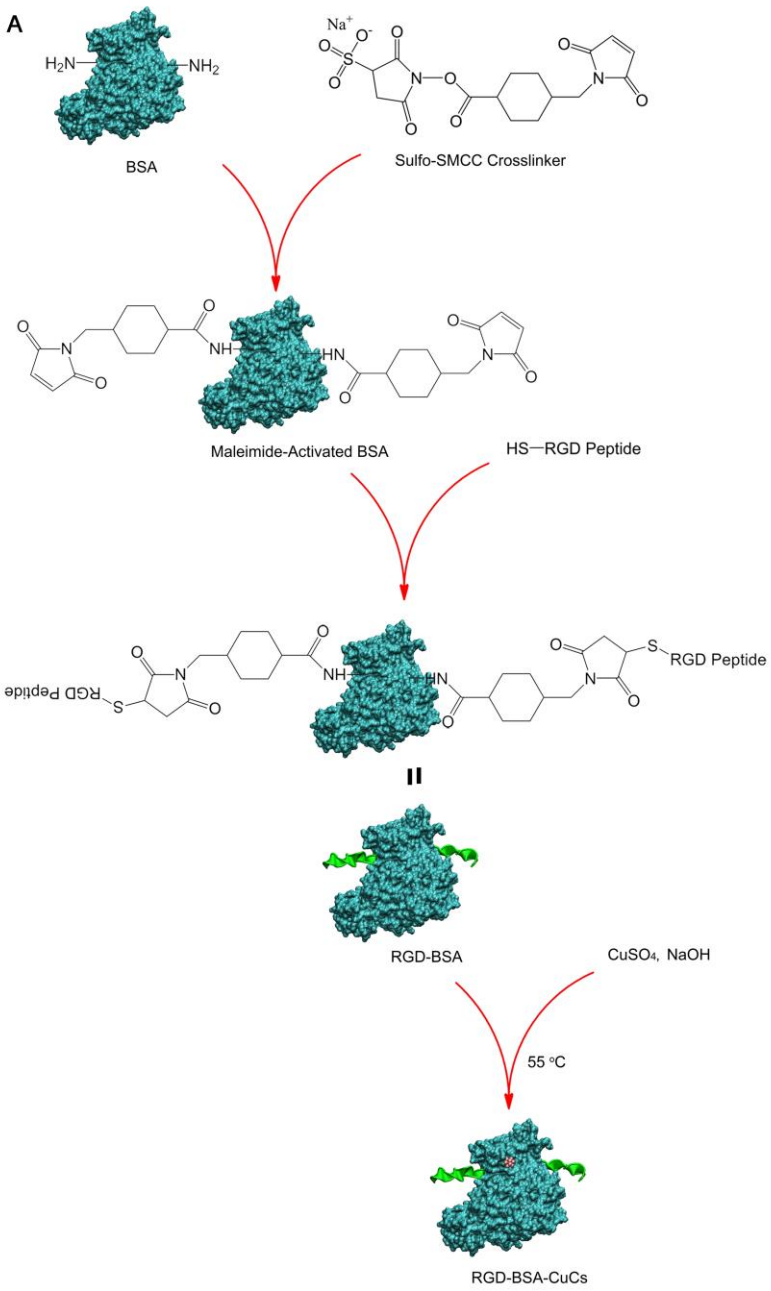

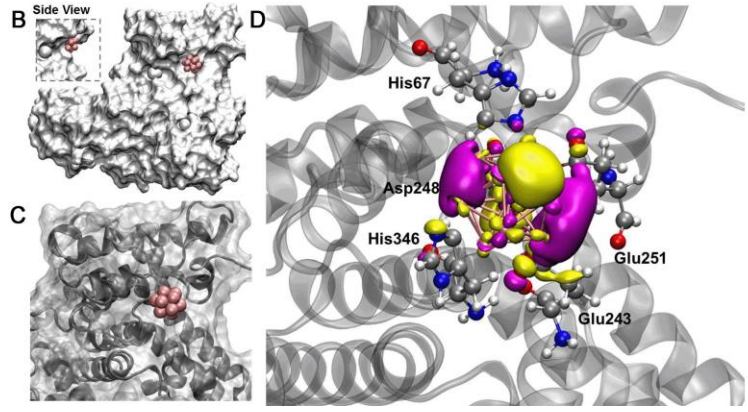

fig. S1. **Schematic illustration of artificial metalloenzyme synthetic strategy and the configuration of Cu_{13} core stuck in BSA by molecular docking calculation.** (**A**) Sulfo-SMCC contains N-hydroxysuccinimide ester and maleimide group that allows covalent conjugation of $–NH_2$ and –SH-containing molecule. Notably, the sequence of the RGD peptide H_2N-CCGPDGRDGRDGRDGR-COOH contains three functional components. The first domain is CC, comprised of –SH group with the ability to link to BSA. Domain two is GP serving as the sequence to avoid steric hindrance. The third domain is DGRDGRDGRDGR, clarified to specifically bounds to integrin $\alpha_v\beta_3$ as a guiding moiety. Then RGD-BSA as template expediently reduces $CuSO_4$ to clusters within cavities of protein under basic pH environment by following an optimized synthetic procedure. (**B**) The insert is the side view of stuck configuration. The Cu_{13} core is in pink, and BSA is in white with iso-surface representation. (**C**) The configuration of Cu_{13} core stuck in BSA with a zoom-in view. BSA is in transparent, and its backbone is in grey. (**D**) The detail configuration of Cu_{13} core chelated by residues of BSA. The electron cloud overlap is indicated in yellow and purple between Cu_{13} core and His67, His346, Asp248, Glu243, Glu251 residues. BSA backbone is in transparent. C, N, O and H atoms are in grey, blue, red, and white, respectively.

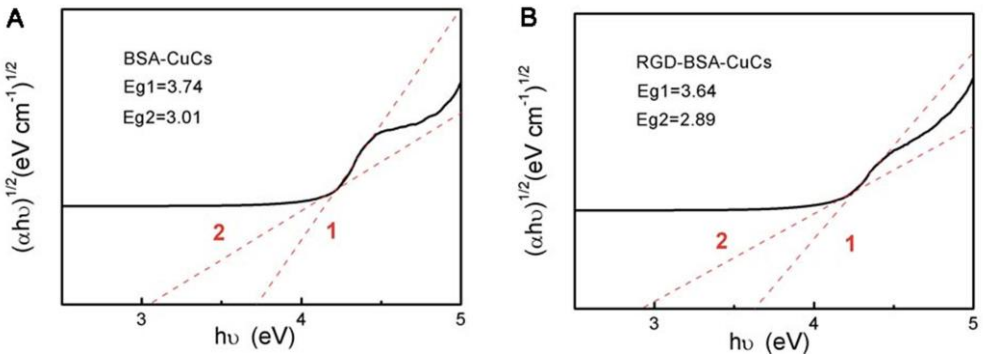

fig. S2. Tauc's plots for ascertaining the direct band gap of BSA-CuCs and RGD-BSA-CuCs.

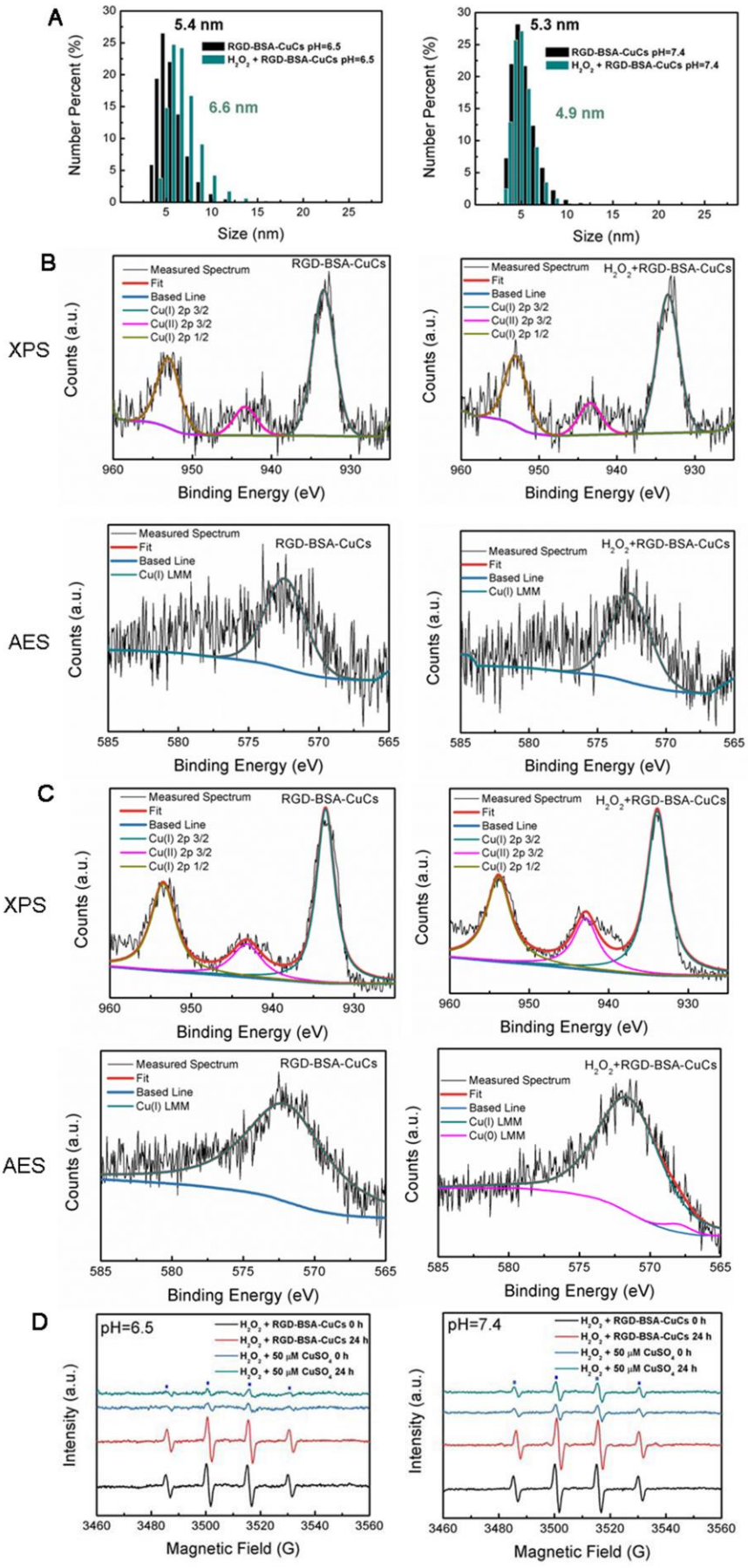
A
5.4 nm
RGD-BSA-CuCs pH=6.5
H2O2 + RGD-BSA-CuCs pH=6.5
6.6 nm
Number Percent (%)
Size (nm)
5.3 nm
RGD-BSA-CuCs pH=7.4
H2O2 + RGD-BSA-CuCs pH=7.4
4.9 nm
B
XPS
Measured Spectrum
Fit
Based Line
Cu(I) 2p 3/2
Cu(II) 2p 3/2
Cu(I) 2p 1/2
RGD-BSA-CuCs
H2O2+RGD-BSA-CuCs
Counts (a.u.)
Binding Energy (eV)
AES
Cu(I) LMM
C
Cu(0) LMM
D
pH=6.5
pH=7.4
H2O2 + RGD-BSA-CuCs 0 h
H2O2 + RGD-BSA-CuCs 24 h
H2O2 + 50 μM CuSO4 0 h
H2O2 + 50 μM CuSO4 24 h
Intensity (a.u.)
Magnetic Field (G)

fig. S3. Hydrated size distribution and oxidation state of RGD-BSA-CuCs before and after the catalysis. (**A**) Hydrated size distributions of RGD-BSA-CuCs at pH 6.5 (left image) and 7.4 (right image) evaluated from DLS results before (black bars) and after (green bars) the catalysis. The catalytic temperature is 37 ^{o}C and duration time is 24 h. (**B**) Representative high resolution XPS spectra of RGD-BSA-CuCs' Cu 2p electrons and corresponding AES spectra of Cu LMM survey discern the oxidation state of Cu clusters, before and after catalysis at pH 6.5. The catalytic temperature is 37 ^{o}C and duration time is 24 h. (**C**) Representative high resolution XPS spectra of RGD-BSA-CuCs' Cu 2p electrons and corresponding AES spectra of Cu LMM survey discern the oxidation state of Cu clusters, before and after catalysis at pH 7.4. The catalytic temperature is 37 ^{o}C and duration time is 24 h. (**D**) ESR spectra of •OH generation in two mixtures (100 μM H_2O_2 and 12 μM RGD-BSA-CuCs, 100 μM H_2O_2 and 50 μM $CuSO_4$) at 37 ^{o}C under pH 6.5 (left image) and pH 7.4 (right image) condition, respectively. The corresponding spectrum is recorded immediately initiation the catalytic reaction or catalytic reaction proceeds for 24 h. Note that 12 μM RGD-BSA-CuCs comprising around 50 μM Cu (II) is determined by the XAFS results.

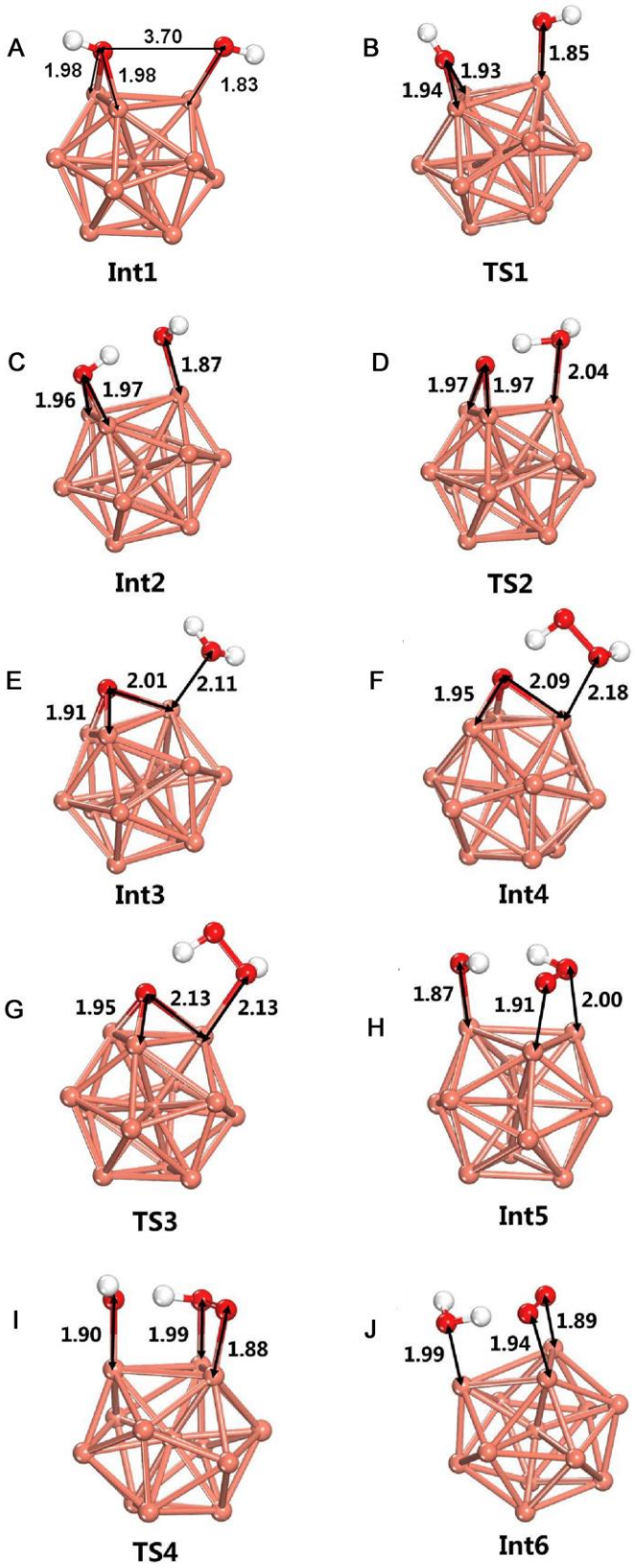

fig. S4. The detailed structure information for all intermediate products and transition states including the key bond lengths. Distances in Å.

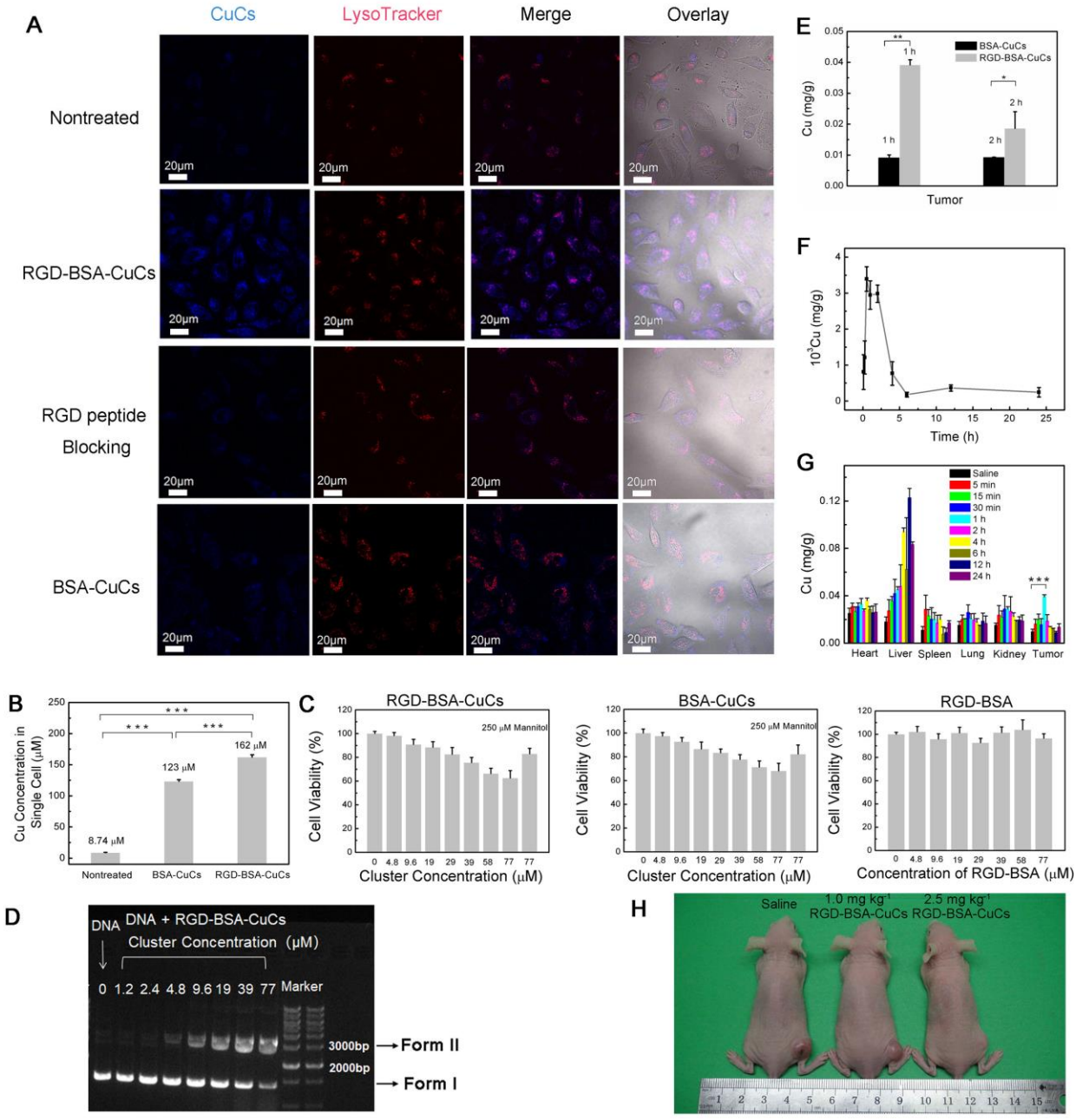

fig. S5. RGD-BSA-CuCs' targeting specificity, therapeutic effect and time-dependent biodistribution. (**A**) Photoluminescence images of A549 cells exposed to LysoTracker Red DND-99 and disperse medium as control (first line); 39 μM RGD-BSA-CuCs for 3 h (second line); 2.0 mM RGD peptide for 1 h, followed by 39 μM RGD-BSA-CuCs (third line); 39 μM BSA-CuCs (fourth line). Note that all above images were collected at the same setting. (**B**) Histograms represent quantitative ICP-MS plots of copper atoms concentration per cell in the case of incubating 19 μM RGD-BSA-CuCs or BSA-CuCs with A549 cells for 24 h, respectively. Inherent Cu ions concentration in untreated single

cell was set as control. Data are shown as mean ± s.d. from three independent experiments. *** denotes $P < 0.001$. (**C**) *In vitro* cell viability of non-cancerous CCC-HPF-1 lung cells after 48 h incubation of RGD-BSA-CuCs *versus* that of BSA-CuCs with the identical Cu concentration. Viability of CCC-HPF-1 cells treated with RGD-BSA is set as control (mean ± s.d., n = 3). (**D**) Agarose gel electrophoretic patterns of supercoiled pUC19 plasmid DNA (20 ng mL^{-1}) in the presence of a series concentration of RGD-BSA-CuCs. The mixture was pre-incubated in pH 7.4 buffer solution at 37 °C for 12 h. (**E**) RGD-BSA-CuCs' *in vivo* targeting capability determined from Cu content analyzed by ICP-MS. A549 cells were inoculated in the flank of nude mice, and mice were treated with 200 μL of RGD-BSA-CuCs or BSA-CuCs at Cu dose of 2.5 mg kg^{-1} through i.p. injection after tumors reached about 100 mm^3. At 1 and 2 h post-injection, mice were sacrificed and tumors were collected, freeze-dried, weighed, digested by mixed acid before Cu content (milligram of Cu per gram of tumor tissue) was analyzed by ICP-MS. Data are shown as mean ± s.d. from three independent experiments. * denotes $P < 0.05$, ** denotes $P < 0.01$. (**F**) Time-dependent Cu concentration (milligram of Cu per gram of blood) variation in the tumor-bearing BALB/c mice's blood after a single i.p. injection of 2.5 mg kg^{-1} RGD-BSA-CuCs. The blood distribution half-life ($t_{1/2\alpha}$) and blood clearance half-life ($t_{1/2\beta}$) of Cu clusters are determined to be 2.0 h and 69 h, respectively, based on the two-compartment model (number of independent mice n = 3, mean ± s.d.). Note that the inherent Cu concentration in blood is subtracted as background value. (**G**) Time-dependent biodistribution of Cu (milligram of Cu per gram of tissues) in main organs and tumors. These organs and tumors were harvested 5 min, 15 min, 30 min, 1 h, 2 h, 4 h, 6 h, 12 h and 24 h after a single i.p. administration of 2.5 mg kg^{-1} RGD-BSA-CuCs to tumor xenograft mice, respectively. Data are shown as mean ± s.d. from three independent experiments. *** denotes $P < 0.001$. (**H**) Representative photograph of tumor-xenografted BALB/c mice after i.p. injection of saline only, RGD-BSA-CuCs at a dosage of 1.0 and 2.5 mg kg^{-1} every two days for 21 days, revealing an efficient inhibition on tumor growth through biocatalysis (Photo credit: Xueyun Gao, Beijing University of Technology).

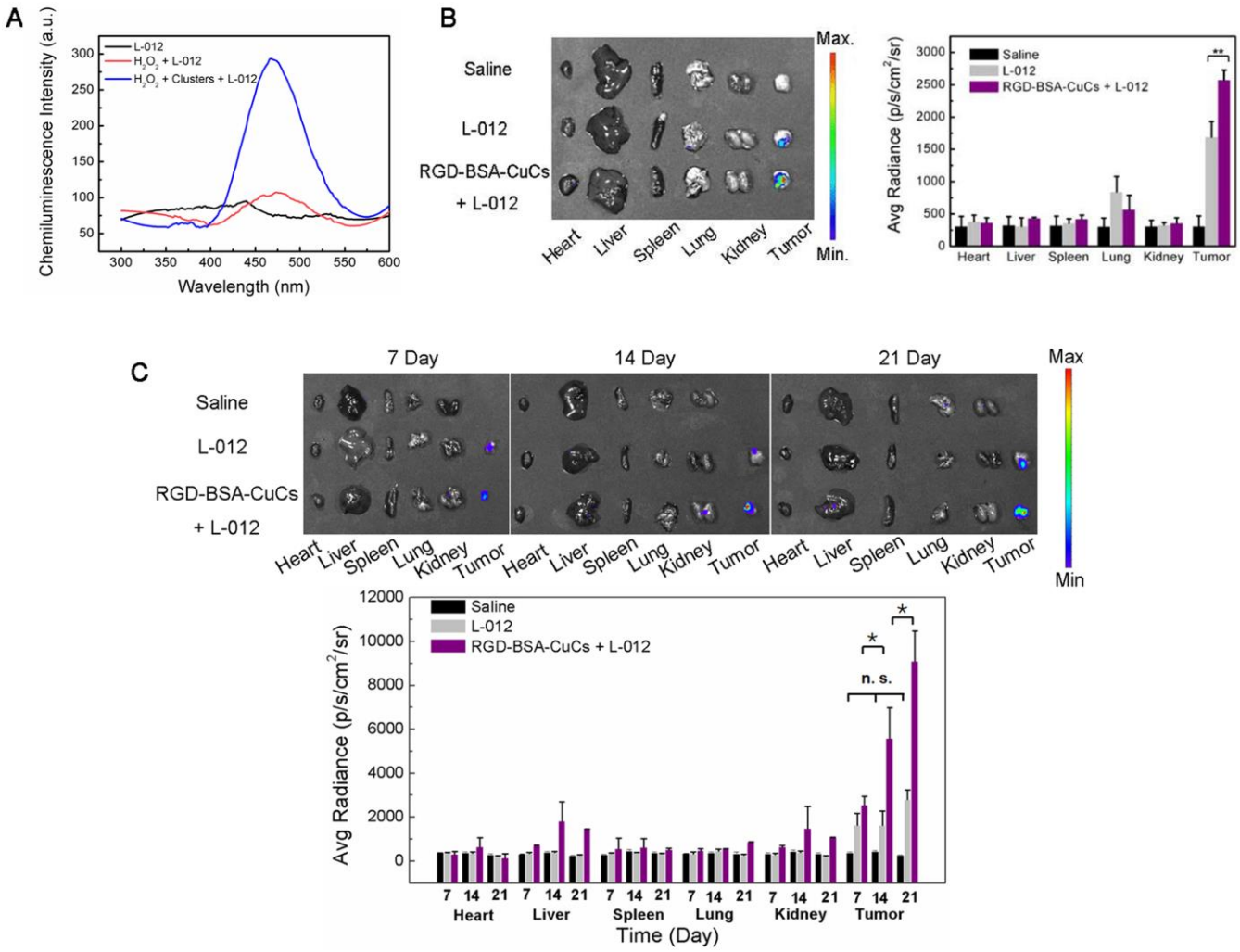

fig. S6. Chemiluminescence spectra of L-012 and representative *ex vivo* chemiluminescent images of dissected major organs and tumors. (**A**) Chemiluminescence spectra of 1.0 mM L-012 in the mixture containing 100 μM H_2O_2 and 77 μM RGD-BSA-CuCs under pH 6.5. The luminescence of control groups was also evaluated, respectively. (**B**) Representative *ex vivo* chemiluminescent image of dissected major organs and tumors to demonstrate signal specifically stems from tumor tissue. At 1 h post-injection (i.p.) of 2.5 mg kg^{-1} RGD-BSA-CuCs, 25 mg kg^{-1} L-012 was i.t. administered to tumor-bearing mice. No detectable chemiluminescence signal are observed from heart, liver, spleen, lung, and kidney of various groups, while a high-intensity chemiluminescence signal is detected in tumor region treated with RGD-BSA-CuCs in addition to L-012 (left image). The pseudo colors represent photons/s cm^2 sr. Right image presents the chemiluminescence intensity in major organs and

tumors at 1 h post-injection (i.p.) of RGD-BSA-CuCs. Data represent the mean ± s.d. of three independent experiments. ** denotes $P < 0.01$. (**C**) Representative *ex vivo* chemiluminescent images of dissected major organs and tumors during 21 days of therapeutic intervention. After mice were i.p. injected with 200 μL of 2.5 mg kg^{-1} RGD-BSA-CuCs for 7, 14, 21 days every other day, 25 mg kg^{-1} L-012 was i.t. administered to mice. Then organs and tumors were harvested and captured after *in vivo* chemiluminescence images were obtained (upper image). The pseudo colors represent photons/s cm^2 sr. The quantitative analysis was conducted as aforementioned (lower image). Data represent the mean ± s.d. of three independent experiments. * denotes $P < 0.05$, n. s. denotes no significance.

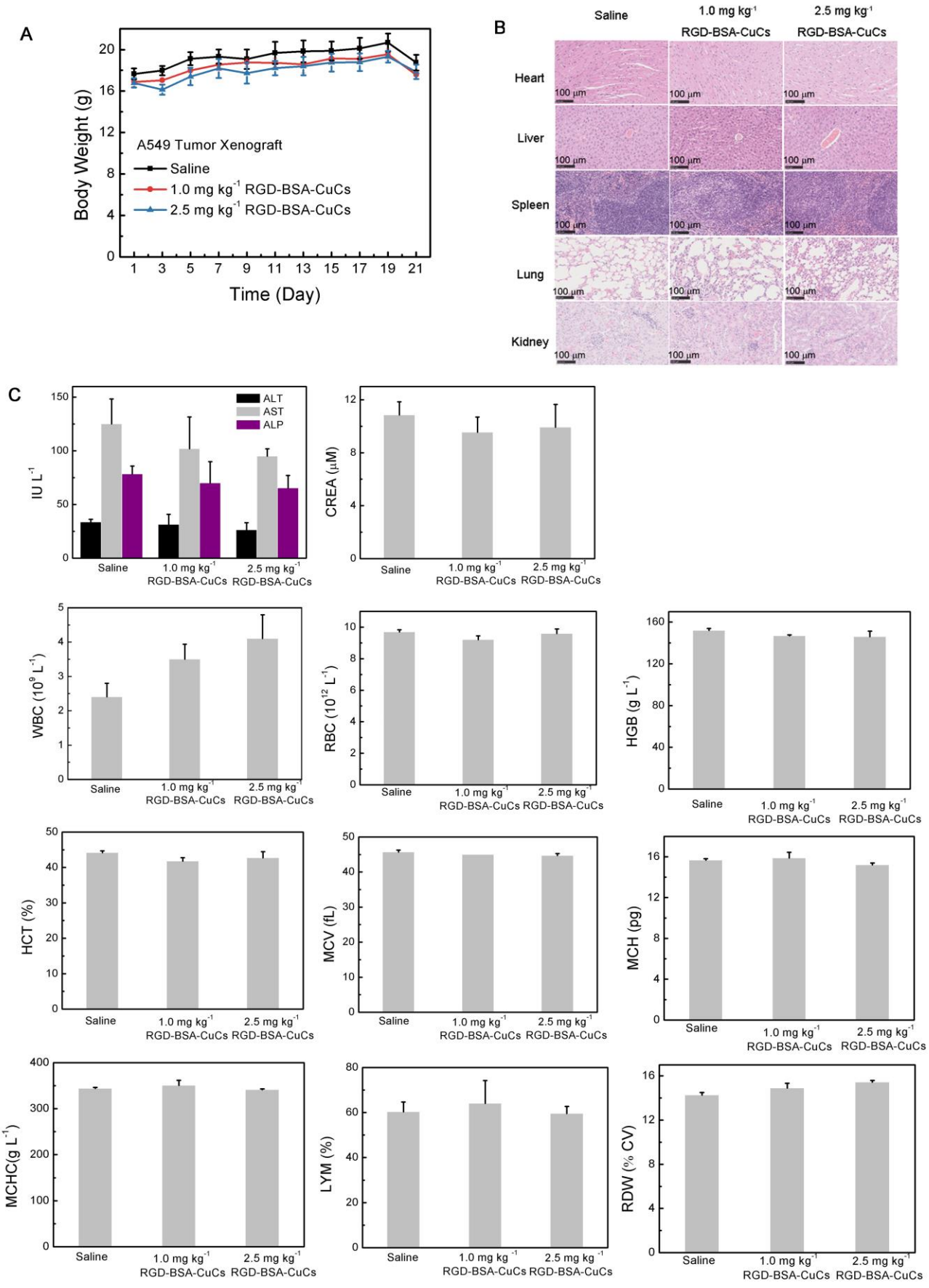

fig. S7. Biosafety assessment of the artificial metalloenzyme. (**A**) The body weight variation of

tumor-bearing mice during treatment, showing no significant fluctuation of body weight in comparison to the saline group. Number of independent BALB/c mice n = 5, mean ± s.d.. (**B**) Pathological H&E staining images of tissue sections from heart, liver, spleen, lung and kidney of BALB/c mice after therapy. The tissue sections were harvested after i.p. injection of 1.0 or 2.5 mg kg^{-1} RGD-BSA-CuCs to mice every 2 days for 21 days. The tissues from mice injected saline was used as control. Clusters behave excellent biocompatibility with invisible organic lesion on main organ tissues. (**C**) Blood biochemical parameters and complete blood counts of BABL/c nude mice after treatment. The liver function related alanine aminotransferase (ALT), aspartate aminotransferase (AST), alkaline phosphatase (ALP), and renal function related creatinine (CREA) indicators present not significant difference compared with control group, suggesting no significant liver and renal function injury. Other hematological indicators, including white blood cell count (WBC), red blood cell count (RBC), hemoglobin (HGB), hematocrit (HCT), mean corpuscular volume (MCV), mean corpuscular hemoglobin (MCH), mean corpuscular hemoglobin concentration (MCHC), lymphocyte (LYM), and red blood cell distribution width-standard deviation (RDW-SD) reveal no significant distinction to the control, confirming the desirable blood safety of the catalyst. Number of independent mice n = 3, mean ± s.d.

Table S1. Comparison of RGD-BSA-CuCs' K_m, V_{max} and K_{cat} under pH 6.5 and 7.4 conditions at 37 ºC. The quantitative analysis was repeated for triplicates.

Catalytic pH Media	K_m [M]	V_{max} [M s^{-1}]	K_{cat} [s^{-1}]
6.5	$(3.87\pm0.17)\times10^{-4}$	$(1.24\pm0.18)\times10^{-9}$	$(1.01\pm0.14)\times10^{-4}$
7.4	$(1.22\pm0.14)\times10^{-3}$	$(7.85\pm0.33)\times10^{-9}$	$(6.38\pm0.27)\times10^{-4}$

Table S2. Atomic ratios of Cu (0), Cu (I) and Cu (II) in RGD-BSA-CuCs pre- and post-catalysis at pH 6.5 or pH 7.4 through XPS and AES analysis. The quantitative analysis was repeated for triplicates.

Samples	Cu (0)	Cu (I)	Cu (II)
Pre-Catalysis, pH 6.5	0%	79±2%	21±2%
Post-Catalysis, pH 6.5	0%	81±4%	19±4%
Pre-Catalysis, pH 7.4	0%	76±2%	24±2%
Post-Catalysis, pH 7.4	1±1%	72±5%	27±4%

Table S3. Atomic ratios of Cu (0), Cu (I) and Cu (II) in RGD-BSA-CuCs pre- and post-catalysis for 24 h under pH 6.5 and 7.4 conditions at 37 ºC through PCA and LCF analysis of XANES spectra. The quantitative analysis was repeated for triplicates.

Samples	Cu (0)	Cu (I)	Cu (II)
Pre-Catalysis, pH 6.5	0%	67±1%	33±1%
Post-Catalysis, pH 6.5	0%	65±4%	35±4%
Pre-Catalysis, pH 7.4	0%	69±1%	31±1%
Post-Catalysis, pH 7.4	0%	66±4%	34±4%